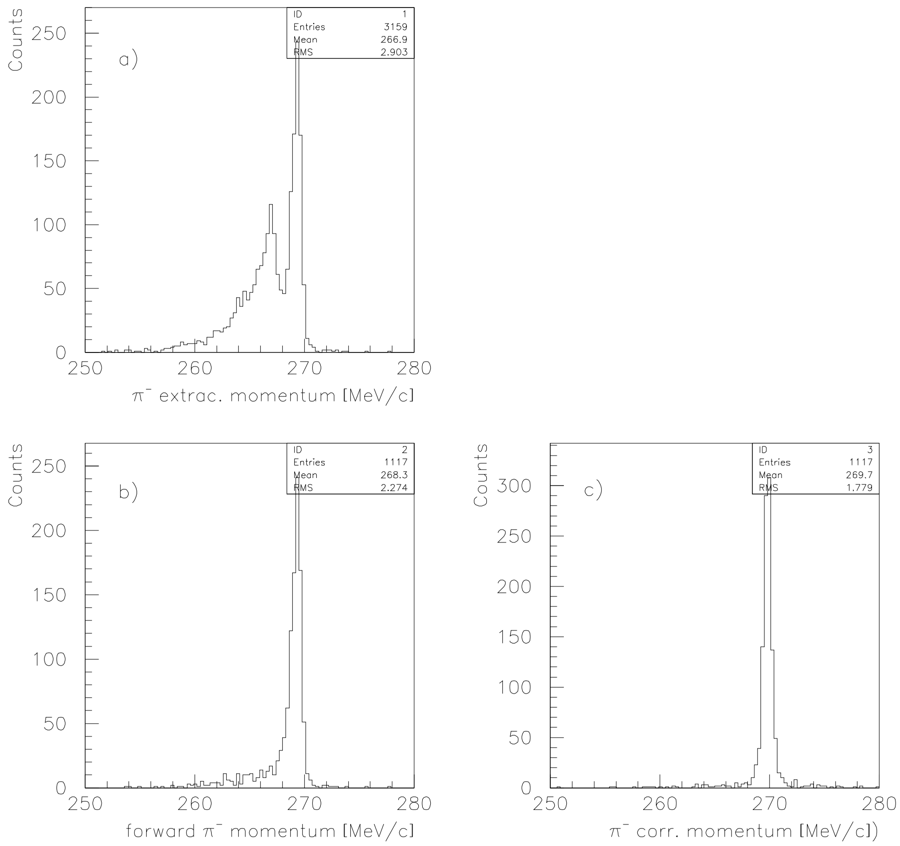

Figure 4: (a) Raw reconstructed momentum distribution of the prompt 270 MeV/c π^-; (b) only forward pions; (c) only forward pions, corrected for the energy loss in the target.

stereo superlayers tested at TRIUMF in December 1994 with a 300 MeV/c pion beam gave $\sim 100\,\mu m$ space resolution with the alternate gas mixtures studied ($Ar-C_2H_6$, $Ar-CO_2$)[24]. Assembly and quality control of about 2700 straw tubes will start at LNF in October 1995, with assembly inside the detector frame starting by March 1996.

Delivery is expected to be complete by November 1995 for all components (scintillators, light guides, and PMT) of the TOFONE array. A 80% efficiency light transmission to the photomultiplier was found by using 90^o conical deflector prisms. A 700 ps time resolution was obtained with a prototype bar.

3.2.3 The Superconducting Solenoid

The magnet contract was signed in December 1993 with Ansaldo, Genova, Italy. Coil and cryostat are expected to be completely assembled in December 1995. The magnet and end-caps will be transported assembled to LNF in June 1996, and installation in the experimental pit is scheduled to begin in mid 1996.

3.3 Performances

The characterization and testing of the FINUDA subdetectors described so far show how the design momentum resolution - the most crucial feature of the detector - is met with a safety margin. To demonstrate the resolving power in hypernuclear spectroscopy, a full simulation was carried out assuming the resolutions in table 3, all amply met, as shown by the test beam results.

Production of a hypernucleus state generating a 270 MeV/c prompt π^- was fully simulated through the detector. The reconstructed raw momentum distribution (fig.4a) shows a shoulder at low energy, due to pions that cross the interaction/target region after being emitted, whose momentum is degraded by the material crossed. When selecting only the 'forward' pions (fig.4b), i.e., those not crossing back over the interaction/target region, the momentum resolution is of the order 0.3% fwhm. However, the momentum resolution for forward prompt pions can be further increased by exploiting the measurement of the K^- stopping point by the ISIM and OSIM, and correcting their momentum by the thickness of target crossed. This is shown in fig.4c, where the mean of the distribution is now set to the 270 MeV/c generated momentum, and the width of the reconstructed spectrum is reduced to 0.25%.

3.4 Triggering Strategies, Rates, and Sensitivities

The FINUDA trigger selects ϕ decays into charged kaons, against decays into $K^o_S K^o_L$, Bhabha scattering, and cosmic rays. Bhabha events are naturally reduced by the geometrical acceptance covered by the TOFINO scintillator array $135^0 \leq \vartheta \leq 45^0$. The trigger requirements exploit the back-to-back topology of the $K^\pm$ pairs, their large $-(dE/dx)$, and the coincidence with the prompt negative pion emitted from the hypernucleus formation as detected by the TOFONE:

- TOFINO back-to-back topology with dE/dx discrimination;
- TOFONE prompt $< 10ns$ coincidence and multiplicity ≥ 1.

The prompt coincidence with TOFONE is dictated by the need to reject μ^+ from K^+ decay. Table 4 shows typical triggering efficiencies for hypernuclear events and residual background contaminations. Hypernucleus formation rates at the initial luminosity $10^{32} cm^{-2} s^{-1}$ are shown in table 4, along with rates for background processes.

The rate of reconstructed hypernuclear events with resolution better than 1 MeV at $\mathcal{L} = 10^{32} cm^{-2} s^{-1}$ is given by the expression:

$$R({}_\Lambda Z) = R_\phi \times BR(\phi \to K^+K^-) \times \frac{N_{{}_\Lambda Z}}{K_{stop}} \times \epsilon_{\pi^-} \times \epsilon_{transp} \simeq 2.5 \times 10^{-2} s^{-1} \simeq 90\, events/hour$$

where $R_\phi = 5 \times 10^2 s^{-1}$, $BR = 0.49$, $N_{{}_\Lambda Z}/K_{stop} = 10^{-3}$ is the capture rate, $\epsilon_{\pi^-} = 13\%$ is the total efficiency for forward (high-resolution) prompt pions, and $\epsilon_{transp} = 80\%$ is the chamber transparency.

The FINUDA rate and resolution capabilities are summarized in table 5.

Table 3: Space, time, and energy resolutions of the FINUDA subdetectors

	Space rms	Time fwhm	Energy fwhm
TOFINO	-	500 ps	$-(dE/dx)$ 50 pe/mip
ISIM,OSIM	50 $\mu m(x,y,z)$	-	$-(dE/dx)$ 20% for K
LMDC	100 $\mu m(x,y)$ 1% wire length (z)	-	-
TOFONE	5 cm (z)	500 ps	-
ST	100 $\mu m(x,y)$ $< 500\mu m(z)$	-	-

Table 4: Efficiency, rejection, and rates for production of hypernuclear states and background processes

Efficiency for hypernucleus production events	
TOFINO BackToBack $\times$ dE/dx threshold	80%
$\times$ TOFONE 10ns prompt coincidence	46%
$\times$ TOFONE ≥ 1 multiplicity (trigger eff. ϵ_T)	39%
$\times$ π^- track has 4 hits	29%
$\times$ forward π^- (eff. ϵ_{π^-})	13%
Background rejection	
Bhabha	$< 10^{-2}$%
$\phi \to K_S K_L$	$(3 \pm 1) \times 10^{-2}$%
$\phi \to \rho\pi$	$(4 \pm 1) \times 10^{-2}$%
$\phi \to \pi^+\pi^-\pi^0$	10^{-2}%
K^- interaction without hypernucleus	7 %
Trigger rates at $10^{32} cm^{-2} s^{-1}$	[Hz]
Hypernucleus production ($10^{-3}/K^-_{stop}$ capture rate)	8×10^{-2}
Bhabha	$< 4 \times 10^{-2}$
$\phi \to K_S K_L$	5×10^{-2}
$\phi \to \rho\pi$	2×10^{-2}
$\phi \to \pi^+\pi^-\pi^0$	10^{-3}
K^- interaction without hypernucleus	15

Table 5: Beam time required (in hours) at $\mathcal{L} = 10^{32} cm^{-2} s^{-1}$ to produce (with 10% and 20% statistical precision) hypernuclear states with capture rates from $10^{-3}/K^-_{stop}$ to $10^{-5}/K^-_{stop}$.

Production rate	10^{-3} 10% st.	10^{-4} 10% st.	10^{-5} 10% st.	10^{-5} 20% st.
S/B=4/1 at 10^{-3}	2.45	96	8000	2000
S/B=8/1 at 10^{-3}	1.8	56	4000	1000
S/B=12/1 at 10^{-3}	1.5	40	2300	575

4 KLOE

The KLOE experiment [2] was proposed in April 1992; approved and funded at the beginning of 1993, construction of the detector began in 1994.

The principal aim of KLOE is the detection of direct CP violation in K^0 decays with a 10^{-4} sensitivity on $\Re(\epsilon'/\epsilon)$. For a comprehensive review see [25] and references therein, while a detailed status report can be found in [26]. More generally, KLOE should be regarded as a precision kaon-interferometer, since by studying the correlations between decays of $K^0_S K^0_L$ pairs, the interference in the decay intensities gives measurements of all eight parameters describing CP and CPT (if any) violations in the neutral kaon system, as described in length by Roberto Peccei at this Symposium [27].

Other physics topics include rare K^0_S decays (10^{10} kaons per year will improve the sensitivity to branching ratios down to the 10^{-8} range), tests of Chiral Perturbation Theories, radiative ϕ decays, and $\gamma\gamma$ physics [28].

To reach the design sensitivity on $\Re(\epsilon'/\epsilon)$, a one-year statistics at full $DA\Phi NE$ luminosity is necessary. It is also necessary to control the detector efficiency for the decays of interest and to reject backgrounds from the copious K^0_L decays to states other than two-pion.

The KLOE detector (fig.5) is a hermetic, 4π geometry apparatus: a cylindrical structure surrounding the beam pipe and consisting of a vertex chamber, a large drift chamber, an electromagnetic calorimeter with state-of-the-art energy and time resolution, and some particle identification, and a superconducting magnet.

4.1 Beam Pipe

A $500 - \mu m$-thick Be beam pipe with spherical shape at the KLOE interaction region is being developed by Brush-Wellman and K-TEK in parallel. The sphere radius (10 cm) is chosen to be much larger than the K^0_S 6-mm decay length.

4.2 Magnet

Rejection of the contamination of the $K^0_L \to \pi^+\pi^-$ sample is possible by measuring momenta with high resolution. Particularly vicious is the background of $K_{\mu 3}$ decays, kinematically overlapping the $\pi^+\pi^-$ decay at 250 MeV/c muon momentum. This overlap decreases as the cube of the magnetic field. On the other hand, tracking efficiency loss is observed when tracks spyralize in a high field. A optimal compromise is found at a 6-kG field generated by a superconducting solenoid [31].

[2] KLOE is on Internet `http://lnfmgr.lnf.infn.it/kloedef.html`

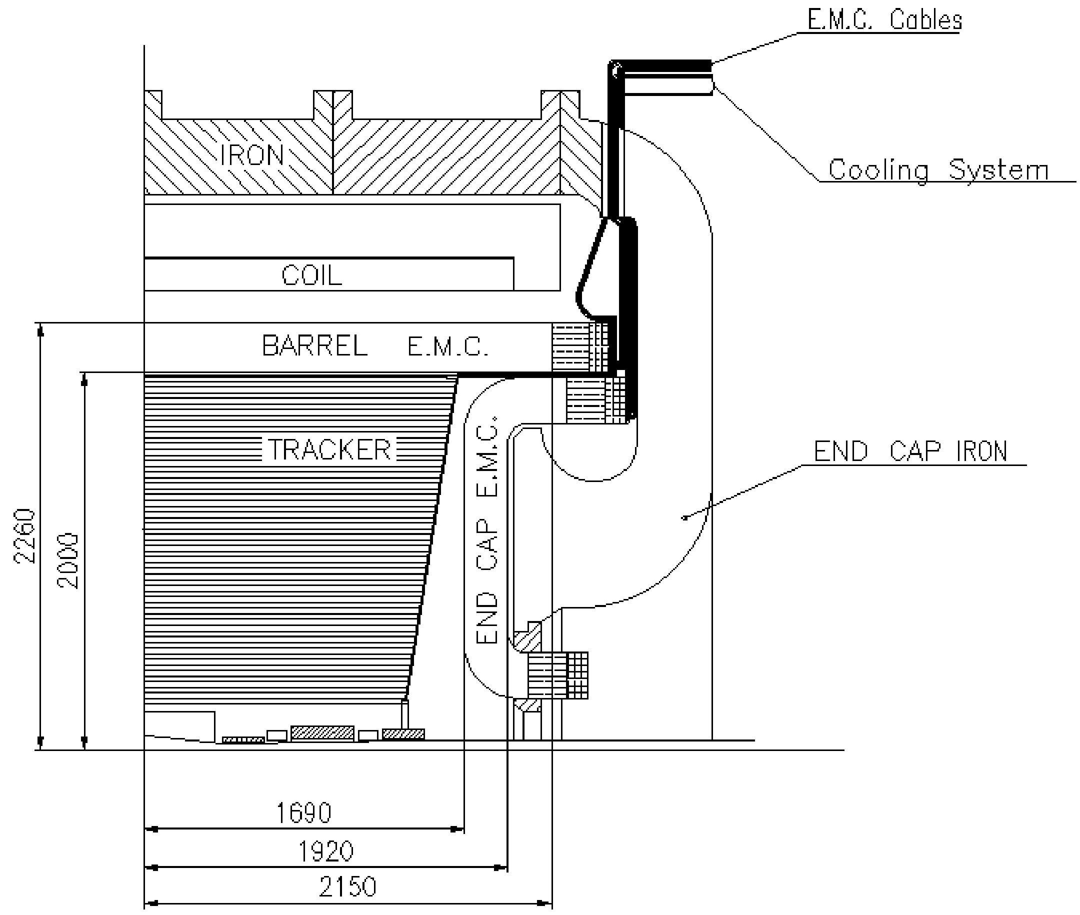

Figure 5: Cross-sectional schematics of the KLOE detector (one quadrant, side view). Dimensions are millimeters.

4.3 Calorimetry

The KLOE calorimeter will reconstruct the $\pi^0\pi^0$ mode, determine the decay vertex space location, reject the $3\pi^0$ decay, and provide π/μ rejection. The technique employed is a Pb-scintillator sampling with 1-mm scintillating fibers embedded in very thin Pb grooved foils. Such a device has been extensively tested [29],[30] and demonstrated to provide good energy resolution, acceptable efficiency for photon energies down to 20 MeV, and spectacular time resolution: the time of arrival of one photon gives the flight path of the K^0 to an accuracy of 0.6 cm at a time resolution of 100 ps. Significant improvements have been achieved recently in the light output of the scintillating fibers [32] and on the photomultiplier [33] quantum efficiency. Eight out of twenty-four modules of the barrel are completed, and the machinery for constructing the endwalls is ready. A cosmic-ray stand is operational at LNF; the design of all the support mechanics is complete.